Journal of Mechanics Engineering and Automation 10 (2020) 140-154
doi: 10.17265/2159-5275/2020.05.002

LES for Turbulent Flows through Ducts of Regular-Polygon Cross-Sections

Masayoshi Okamoto

Graduate School of Integrated Science and Technology, Shizuoka University, Hamamatsu 432-8561, Japan

Abstract: In this study, a large eddy simulation (LES) for fully-developed turbulent flows through a duct of regular-polygon cross-section using the immersed boundary (IB) method is performed. In case of the turbulent flow through the square duct, though there are some disagreements of the mean quantities related with the streamwise velocity among the present LES, the previous direct numerical simulation (DNS) and the LES without the IB method, and the present LES can reproduce the secondary flow of the DNS and LES. The LES result for ten types of regular-polygon duct shows that the secondary-flow speed decreases as the number of sides of the regular polygon *n* increases and that the secondary flow in case of the regular icosagon duct disappears like the turbulent pipe flow. In case of low *n*, the behavior of the turbulent structures near the side center is different from that near the vertex.

Key words: Turbulence, secondary flow, regular polygonal duct, LES, IB method.

1. Introduction

The flow through the ducts is very important in the engineering and the ducts are roughly classified into the circular pipe and the rectangle duct according to geometry. In the laminar flow, there is no large difference of the profile of the streamwise velocity between the geometric shapes of the duct cross-sections and no flow perpendicular to the streamwise flow occurs. On the other hand, in the turbulent flow through the square duct, the mean velocity in the cross section occurs due to the streamwise driving force as well as the streamwise mean velocity unlike the turbulent pipe flow. This cross-section flow is called Prandtl's secondary flow of the second kind and is caused by the anisotropy of the Reynolds stress [1, 2]. The secondary flows have been studied to research the effect on river bottoms and channels in the civil engineering. We have also performed the direct numerical simulation (DNS) for the turbulent flow in square ducts adding system rotation and compressibility effects [3-5]. However, the flows through the ducts with the cross section except the quadrangle have been little studied.

Thus, in this study, for the purpose of examining how the secondary flow changes with geometric shapes of the cross section other than squares, we perform numerical simulations for the turbulent flows through the ducts with nine types of regular-polygonal cross-section and pipe. The cross-section shapes adopted in this calculation are regular triangle, square, pentagon, hexagon, heptagon, octagon, decagon, dodecagon, icosagon. However, in these flow-fields, it is not possible to construct a grid system whose lines are orthogonal except for regular square and circular cross-sections, and it is difficult to perform an exact simulation like DNS that needs the high accuracy scheme. Therefore, we perform the large eddy simulation (LES) combined with the immersed boundary (IB) method proposed by Goldstein et al. [6] for the fully-developed turbulent flow through the regular-polygon ducts. In this LES, the cross section of the regular polygonal duct is reproduced by the IB method with the uniform orthogonal grid-system. In this paper, after testing the prediction ability of this LES-IB code in comparison with the DNS and the LES without the IB method, we will examine the

Corresponding author: Masayoshi Okamoto, doctor of science, associate professor, research fields: physics, mathematics, fluid mechanics, turbulence statistical theory.

dependency of the secondary flow on the number of sides of the regular polygon by the present LES results.

2. Analytical Equation

The analytical equations in the eddy-viscosity-type LES and the IB method are written by

$$\frac{\partial \bar{u}_i}{\partial t} + \frac{\partial \bar{u}_j \bar{u}_i}{\partial x_j} = \frac{\partial}{\partial x_j}\left\{2\left(\nu + \nu_{SGS}\right)\bar{s}_{ij}\right\} - \frac{\partial \bar{p}}{\partial x_i} + f_i + g_i \quad (1)$$

$$\frac{\partial \bar{u}_j}{\partial x_j} = 0 \quad (2)$$

Here, $\bar{u}_i$ is the grid-scale (GS) velocity, $\bar{p}$ is the GS pressure divided by the constant density, ν is the molecular viscosity, and ν_{SGS} is the subgrid-scale (SGS) eddy viscosity. In this study we adopt the coherent-structure Smagorinsky model proposed by Kobayashi [7] as the SGS model. This model has a great merit that we can carry out the LES without wall-damping function and tuning the model constant, and the SGS eddy-viscosity is modeled by

$$\nu_{SGS} = C\left|\frac{Q_2}{E}\right|^{3/2}\Delta^2\bar{s} \quad (3)$$

Here, Δ is the subgrid characteristic length scale, Q_2 is the second invariance of the GS velocity gradient, E is the magnitude of the GS velocity gradient tensor, $\bar{s}$ is the magnitude of the GS strain tensor $\bar{s}_{ij}$. The definitional identities of these quantities are expressed by

$$Q_2 \equiv -\frac{1}{2}\frac{\partial \bar{u}_i}{\partial x_j}\frac{\partial \bar{u}_j}{\partial x_i}, \quad E \equiv \frac{1}{2}\frac{\partial \bar{u}_i}{\partial x_j}\frac{\partial \bar{u}_i}{\partial x_j}, \quad \bar{s} \equiv \sqrt{2\bar{s}_{ij}\bar{s}_{ij}},$$

$$\bar{s}_{ij} \equiv \frac{1}{2}\left(\frac{\partial \bar{u}_i}{\partial x_j} + \frac{\partial \bar{u}_j}{\partial x_i}\right) \quad (4)$$

C is the fixed model constant, 0.05. f_i is a constant driving force in the streamwise direction and its magnitude f_n is dependent on the number of sides of regular polygon, n. Thus, using n, we express the driving force by $f_i = f_n\delta_{i1}$. The last term g_i in Eq. (1) is the restoring force for the solid body in the fluid according to the IB method proposed by Goldstein et al. [6] and is given by

$$g_i(\mathbf{x},t) = -\gamma(\mathbf{x})\left(\alpha u_i(\mathbf{x},t) + \beta\int_0^t dt' u_i(\mathbf{x},t')\right) \quad (5)$$

where α and β are positive free-parameters, 200 and 5, respectively. The function γ means the ratio of the solid volume to the lattice one defined at $\mathbf{x}$ and $0 \le \gamma \le 1$.

3. Flow Field and Numerical Scheme

In this section, we explain the mathematical property of the regular polygonal with n sides. In its circumscribed circle, the central angle for a side, ϕ_n, is $2\pi/n$. Using the cross-section area S_n, the radius of the circumscribed circle, r_n, is expressed by

$$r_n = \sqrt{\frac{2S_n}{n\sin\phi_n}} \quad (6)$$

As an example, Fig. 1 shows the calculation domain and the regular-pentagon duct. A top point is placed on the positive y axis and the coordinates of all vertices are written by

$$P_k = \left(r_n\sin k\phi_n, r_n\cos k\phi_n\right) \quad (7)$$

with k = 0, 1, ···, n-1. The length of the side l_n is

$$l_n = 2\sqrt{\frac{S_n}{n}\tan\frac{\phi_n}{2}} \quad (8)$$

The limit of r_n as n approaches infinity is $r_\infty = \sqrt{S_\infty/\pi}$ and the regular polygonal corresponds to a circle.

In this study, the Reynolds number defined by the global friction velocity $u_\tau = \sqrt{\bar{\tau}_x}$ as a characteristic velocity and the square of the cross-section area S_n as a characteristic length is fixed as 400. The bulk-level balance equation of force is

$$0 = -nl_n\bar{\tau}_x + S_n f_n \quad (9)$$

The driving force is dependent on n as follows

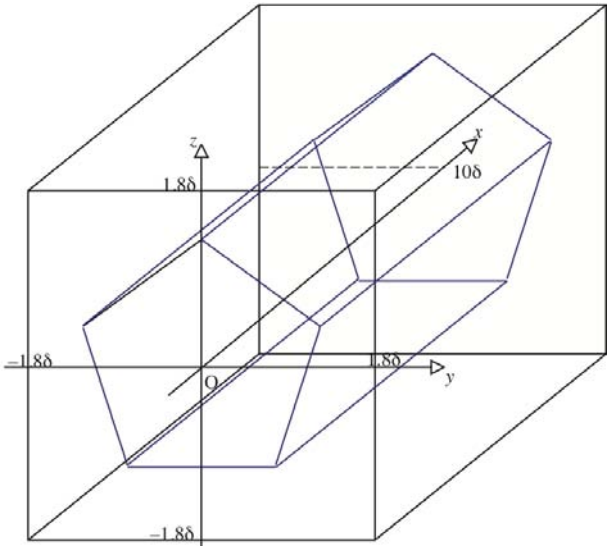

Fig. 1 Flow configuration and coordinate system.

$$f_n = 2\overline{\tau}_x \sqrt{\frac{n}{S_n} \tan\frac{\phi_n}{2}} \tag{10}$$

On the condition that $S_n = 4$ and $\overline{\tau}_x = 1$, the maximum value of the force is $f_3 = 3^{3/4} \approx 2.28$ at $n = 3$ and as n increases the force is monotonously weakened into the circular value $f_\infty = \pi^{1/2} \approx 1.77$. The difference between the driving forces of a circle duct and a dodecagon duct is 1.28% and the force of an icosagon one is very close to that of a circle one.

In this LES, we use the numerical scheme with the conservative second-order central difference as the spatial discretization, the second-order Adams-Bashforth method as the time integration method and the direct method combined with the fast-Fourier transformation analysis in x and z directions and the tridiagonal matrix one in y direction as the pressure solver. The calculation domain is 10 × 3.6 × 3.6, which can include all regular polygonal, and a center of balance is matched with the origin of the coordinate. Thus, a considerable number of grid points located away from the center of balance are in the solid-wall region and the virtual force acts there in the IB method. It is necessary to set up fine-resolution grids near the wall in LES and the cross section of the regular polygonal duct is resolved using a great number of uniform grids. We perform the present LES with 64 × 512 × 512 and the grid resolution for the cross section is about 1.4. In order to check the grid dependency, we also simulate the LES with the IB method by coarse grid system, 64 × 256 × 256, and it is confirmed that the difference between both results is small.

The mean quantities are estimated by taking the spatial average in the homogeneous x direction and the time average, and moreover those values are calculated according to the symmetry of regular polygons. In this symmetry analysis we utilize the coordinate transformation from Cartesian coordinate system and cylindrical one.

4. Verification of the Present LES-IB Code

Before examining the present result of the regular-polygonal duct case, in order to check the present LES code, we compare the result in a turbulent flow through a square duct at Re = 400 with those of the previous DNS [8] and the LES without the IB method. The LES is performed with the nonuniform grid system 64^3 and the same SGS model [7]. Fig. 2 shows the streamwise mean velocity U and the streamlines of the secondary flow. In this figure, we rotate the results of the DNS and LES without the IB method by π/4. There are good agreements of the distribution pattern among those results, but the streamwise mean velocity of the present LES is underpredicted in comparison with the DNS and LES. On the other hand, the maximum values of the secondary flow are 0.309 in DNS, 0.321 in LES and 0.346 in LES with the IB method and the present LES can reproduce the secondary flow of DNS.

Next, let us compare the distribution of the Reynolds stresses. The coordinate system used by the DNS and LES without the IB method is rotated by π/4 with respect to that of the present LES. Therefore, we transform the Reynolds stresses $\langle u_i' u_j' \rangle^O$ of the DNS and LES to those $\langle u_i' u_j' \rangle^N$ in the present coordinate system as follows.

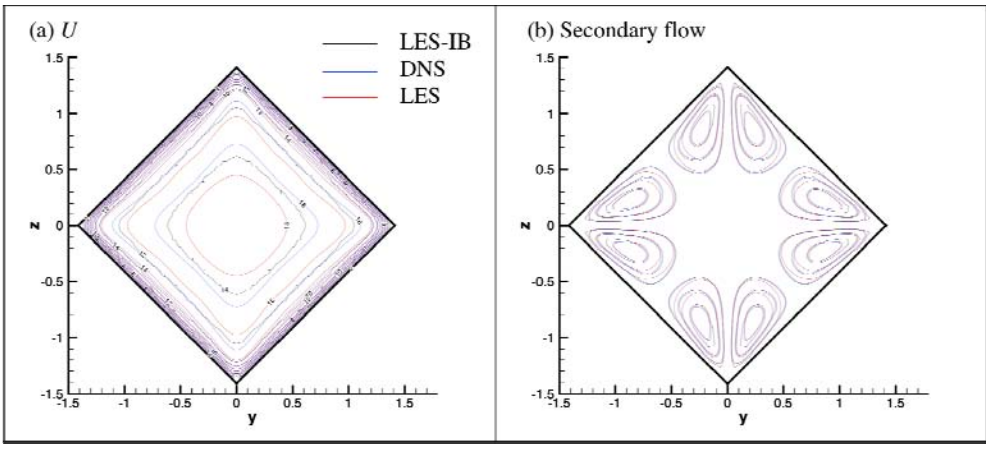

Fig. 2 Contour of the mean streamwise velocity and streamlines of the secondary flow.

$$\langle u'u' \rangle^N = \langle u'u' \rangle^O \tag{11}$$

$$\langle v'v' \rangle^N = \frac{1}{2}\left(\langle v'v' \rangle^O + 2\langle v'w' \rangle^O + \langle w'w' \rangle^O \right) \tag{12}$$

$$\langle w'w' \rangle^N = \frac{1}{2}\left(\langle v'v' \rangle^O - 2\langle v'w' \rangle^O + \langle w'w' \rangle^O \right) \tag{13}$$

$$\langle u'v' \rangle^N = \frac{\sqrt{2}}{2}\left(\langle u'v' \rangle^O + \langle w'u' \rangle^O \right) \tag{14}$$

$$\langle v'w' \rangle^N = \frac{1}{2}\left(-\langle v'v' \rangle^O + \langle w'w' \rangle^O \right) \tag{15}$$

$$\langle w'u' \rangle^N = \frac{\sqrt{2}}{2}\left(-\langle u'v' \rangle^O + \langle w'u' \rangle^O \right) \tag{16}$$

Taking into account the π/2 rotational symmetry, the four elements of the Reynolds stresses are shown in Fig. 3. Although there is good agreement of the distribution

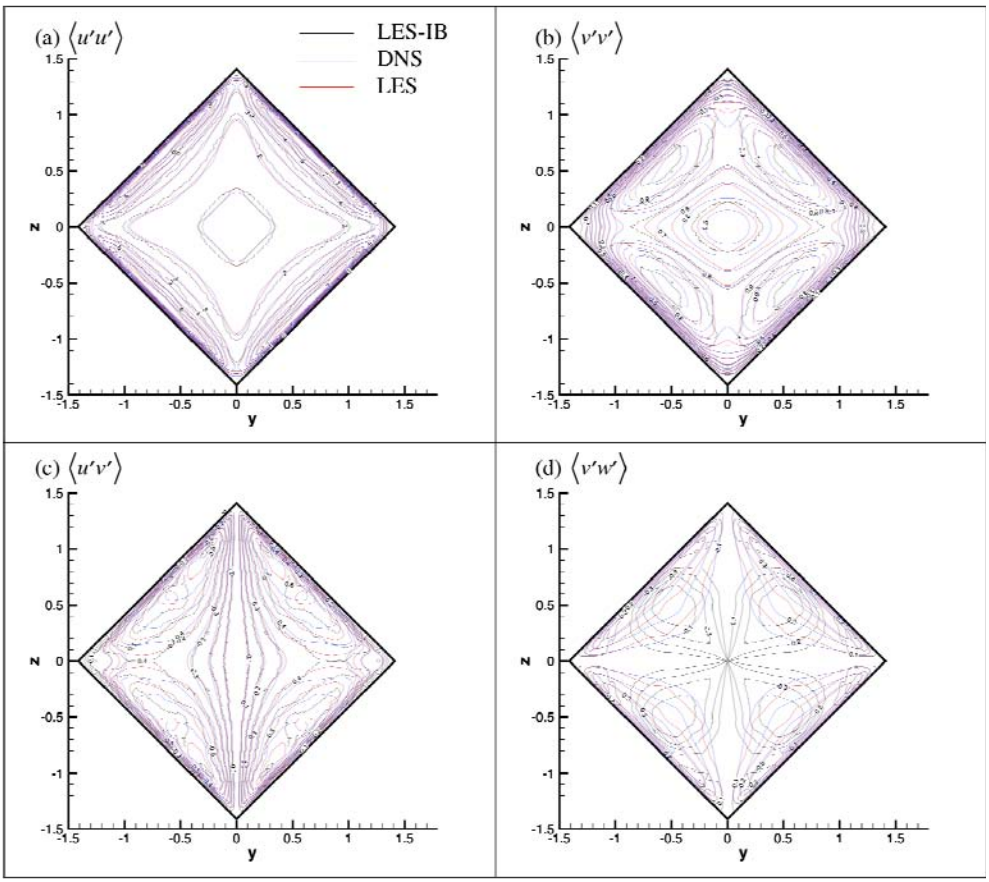

Fig. 3 Distributions of the Reynolds stresses.

shape of $\langle u'u' \rangle$ among all three simulation-results, the present LES has a maximum value of about 6, which is smaller than about 8 of the maximum one in DNS and LES without the IB method. The present LES with the IB method underpredicts $\langle u'u' \rangle$ like the streamwise mean velocity. On the other hand, the present LES can properly reproduce $\langle v'v' \rangle$ and $\langle u'v' \rangle$ of DNS and LES. However, explaining in detail, the positions of the $\langle v'v' \rangle$ maximum value are slightly shifted near the top and bottom vertices and those of $\langle u'v' \rangle$ are displaced to the left and right ones. The distribution of $\langle v'w' \rangle$ in the present LES is not similar to those in DNS and LES. The present LES is able to reproduce plus or minus sign in each quadrant, but has a large value away from the wall.

The above results indicate that the present LES with the IB method does not have sufficient prediction ability to evaluate rigorous physical phenomena, however, the qualitative investigation focusing on the behavior of the secondary flows in the regular-polygonal ducts is allowed. In addition, this inadequate prediction ability seems to be due to the IB method rather than the SGS model.

5. Numerical Result

First, the dependency of the number of sides n between the bulk velocity U_B and the maximum secondary velocity V_{max} is shown in Fig. 4. As already mentioned in previous section, U_B in the present LES is about 12.5 and small. As n increases, U_B slightly increases by about 1.6%. On the other hand, it can be confirmed that V_{max} monotonously decreases to zero in the turbulent pipe flow as n increases. In comparison with V_{max} of the equilateral-triangle duct, V_{max} of the regular-decagon duct is about half, and V_{max} of the regular-icosagon duct is reduced to about 10%. The n dependence can be decomposed into two parts at $n = 8$. In the region of small n, V_{max} gently decreases by $n^{-0.337}$ and in the large region, rapidly decreases by $n^{-2.47}$.

The results of the streamwise mean velocity U and secondary flow are shown in Fig. 5. The colored

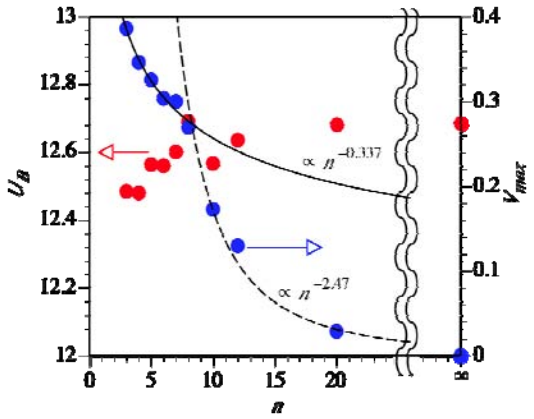

Fig. 4 Bulk velocity U_B and maximum velocity of the secondary flow V_{max}.

contour chart indicates the distribution of the streamwise mean velocity and the uncolored one represents the streamlines of the secondary flow. The contour interval between the contour lines is equal in all cases. In the cases of the regular-triangle and square ducts, the cross-sectional shape has a great influence on the high-speed contour lines of U in the duct center. However, as n increases, more and more contour lines become circular. In particular, the distribution of a regular dodecagonal duct is very close to that of a circular pipe. Next, focusing on the secondary flows, $2n$ circulating flows appear in the cross section up to $n = 12$ and the secondary flow is not generated in the regular-decagonal and circular ducts. Assuming the symmetry on the mean quantities, there is a pair of cyclonic and anticyclonic circulating flows in a triangle consisting of any one side and two segments connecting its edge-points with a median point. The secondary flow in the equilateral triangle and regular square is very strong and its circulating flows extends to the center of the duct. As n increases, the area reached by the contour lines of the circulating flow becomes smaller near the vicinity of the wall, and the magnitude of the secondary flow decreases. Since the convection effect of the secondary flow weakens in the large n case, the overhang of the distribution in the streamwise mean velocity to vertices disappears. As a result of this LES, the turbulent flow through the regular-polygonal ducts with $n \geq 20$ is very close to that in the pipe.

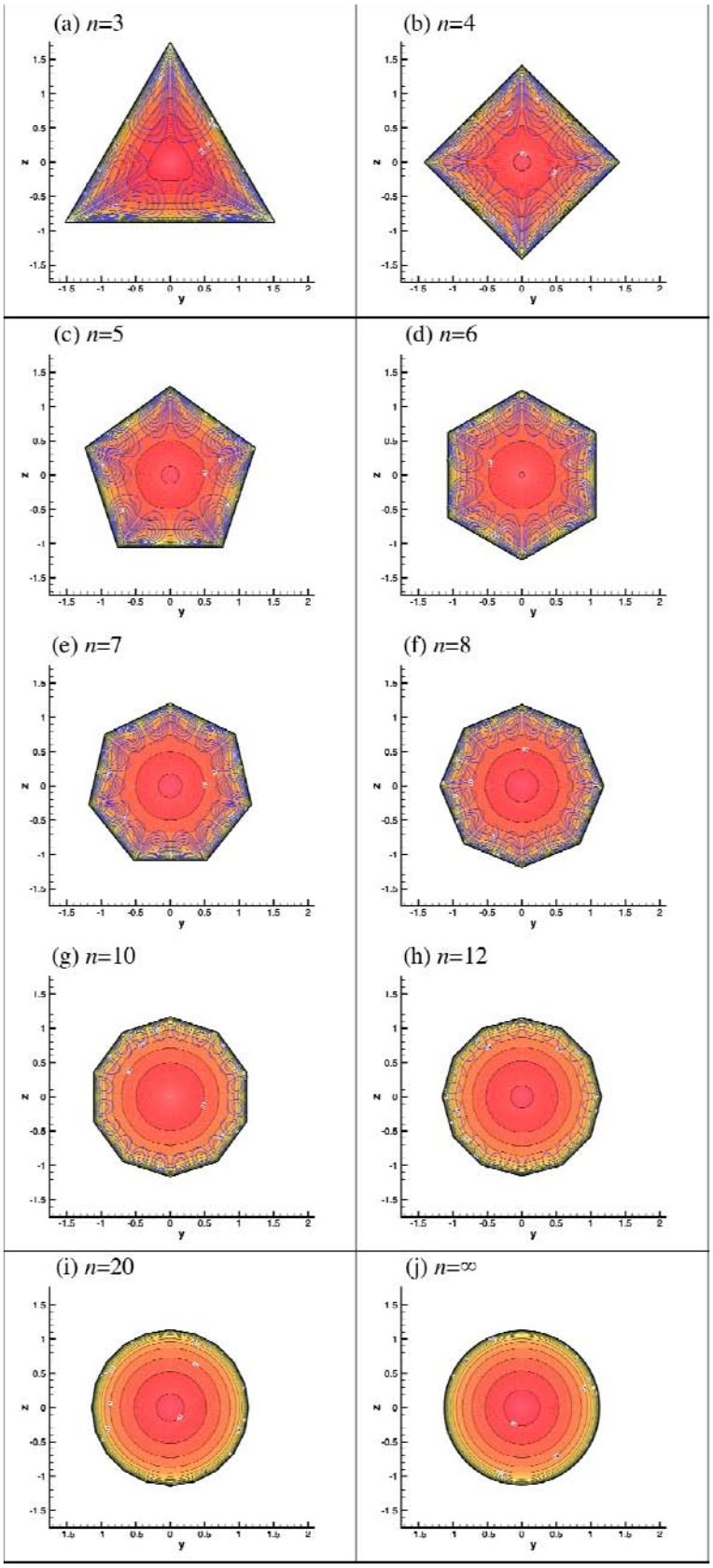

Fig. 5 Streamwise mean velocity *U* and secondary flow.

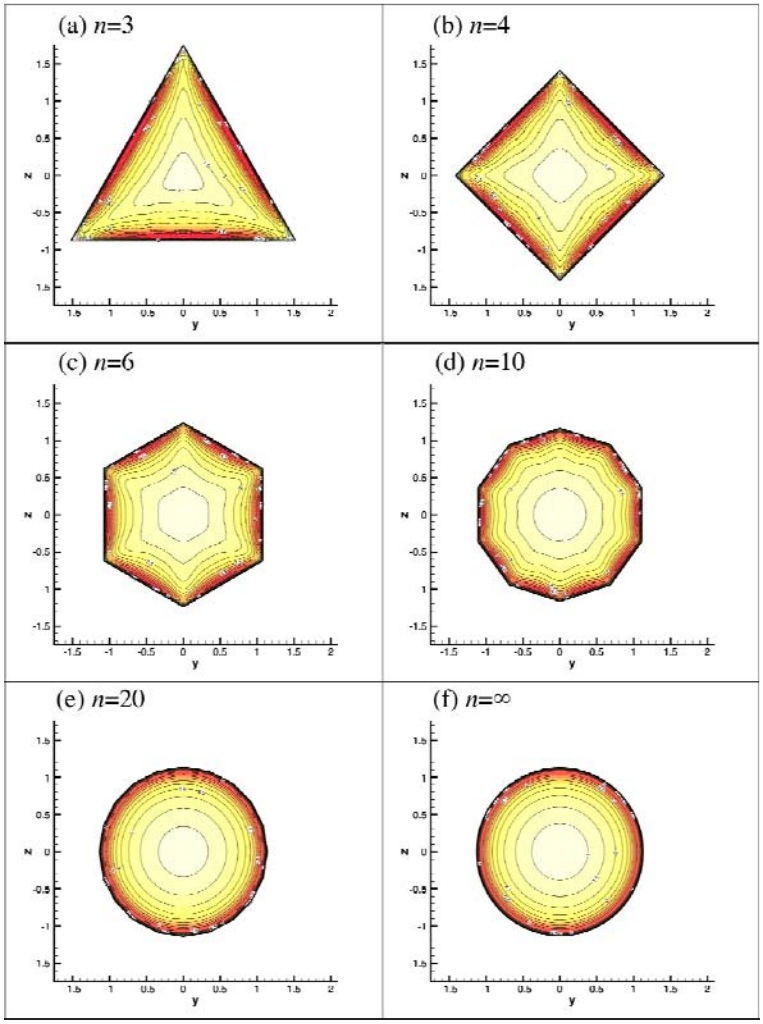

Fig. 6 Reynolds normal stress $\langle u'u' \rangle$.

Fig. 6 is the distributions of Reynolds normal stress $\langle u'u' \rangle$ and the high values are found at positions near the middle of each side. The influence of the cross-section shape is more apparent in $\langle u'u' \rangle$ than in the streamwise mean velocity. In Fig. 7, the vertical component $\langle v'v' \rangle$ becomes high near the parallel or gentle slope sides to the horizon and small near the vertices. In the circular-pipe case, this quantity has a vertical symmetry and is large near the top and bottom. The distribution in the regular-decagon duct is very similar to that in the circle duct. When n is a multiple of 4, the distribution of $\langle v'v' \rangle$ matches that with $\langle w'w' \rangle$ rotated by $\pi/2$ from the symmetry of the regular polygon. In Fig. 8, we compares the vertical and horizontal stress components $\langle v'v' \rangle$ and $\langle w'w' \rangle$ for the case with odd n for which this symmetry is broken. The distribution of $\langle v'v' \rangle$ is very close to that of $\langle w'w' \rangle$ near the lower slope-wall in the regular-heptagon duct. This cause is that the angle between the lower side and horizon is close to $\pi/4$ and that the length of the side of the regular-heptagon duct is shorter than that of the square duct in which the distribution is asymmetric with respect to the midpoint of the side.

Next, we put a focus on the Reynolds shear stresses. $\langle u'v' \rangle$ and $\langle w'u' \rangle$ are related to the streamwise mean velocity and $\langle v'w' \rangle$ has an influence on the secondary flow. The results of the primary shear stress $\langle u'v' \rangle$ are given in Fig. 9. $\langle u'v' \rangle$ tends to be very large near the side wall with $z = 0$. In particular, the result of the

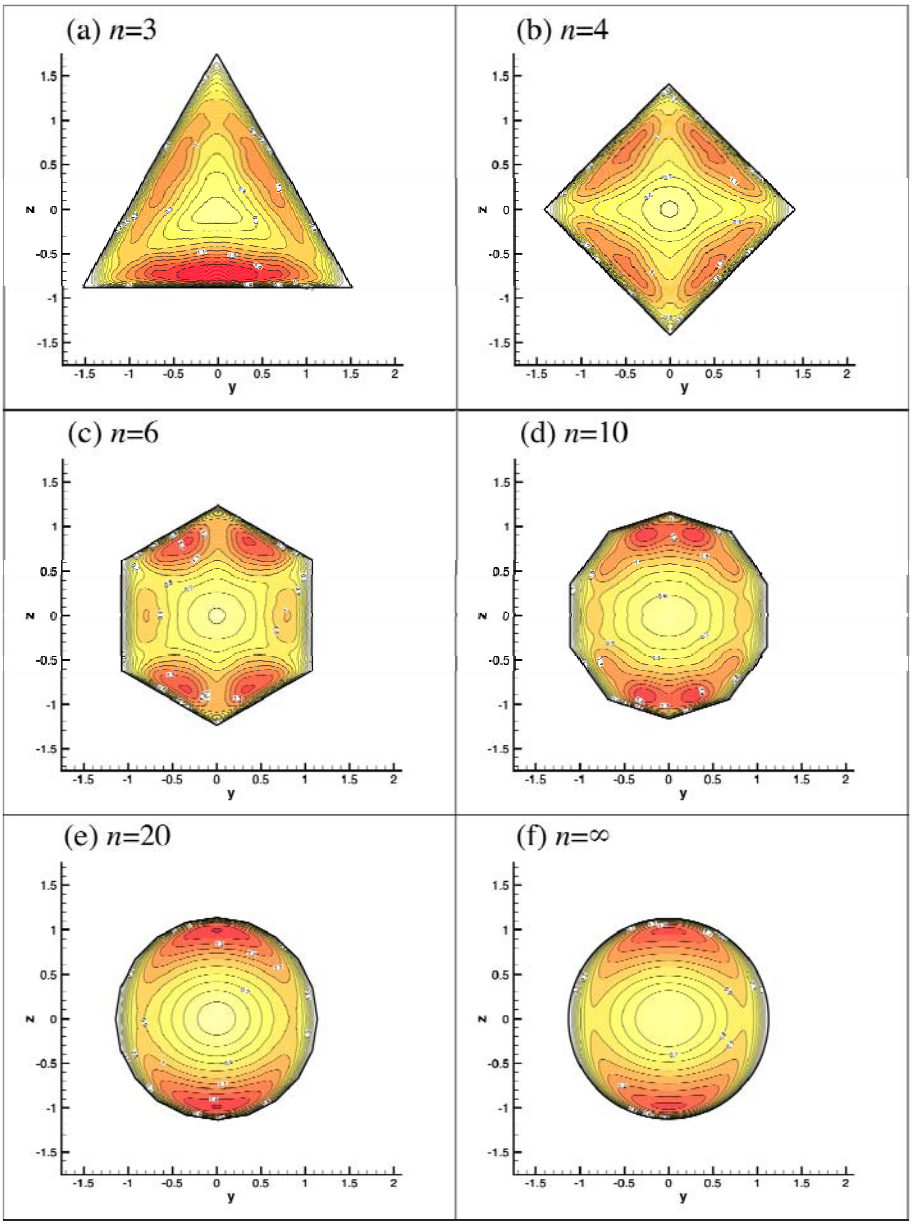

Fig. 7 Reynolds normal stress $\langle v'v' \rangle$.

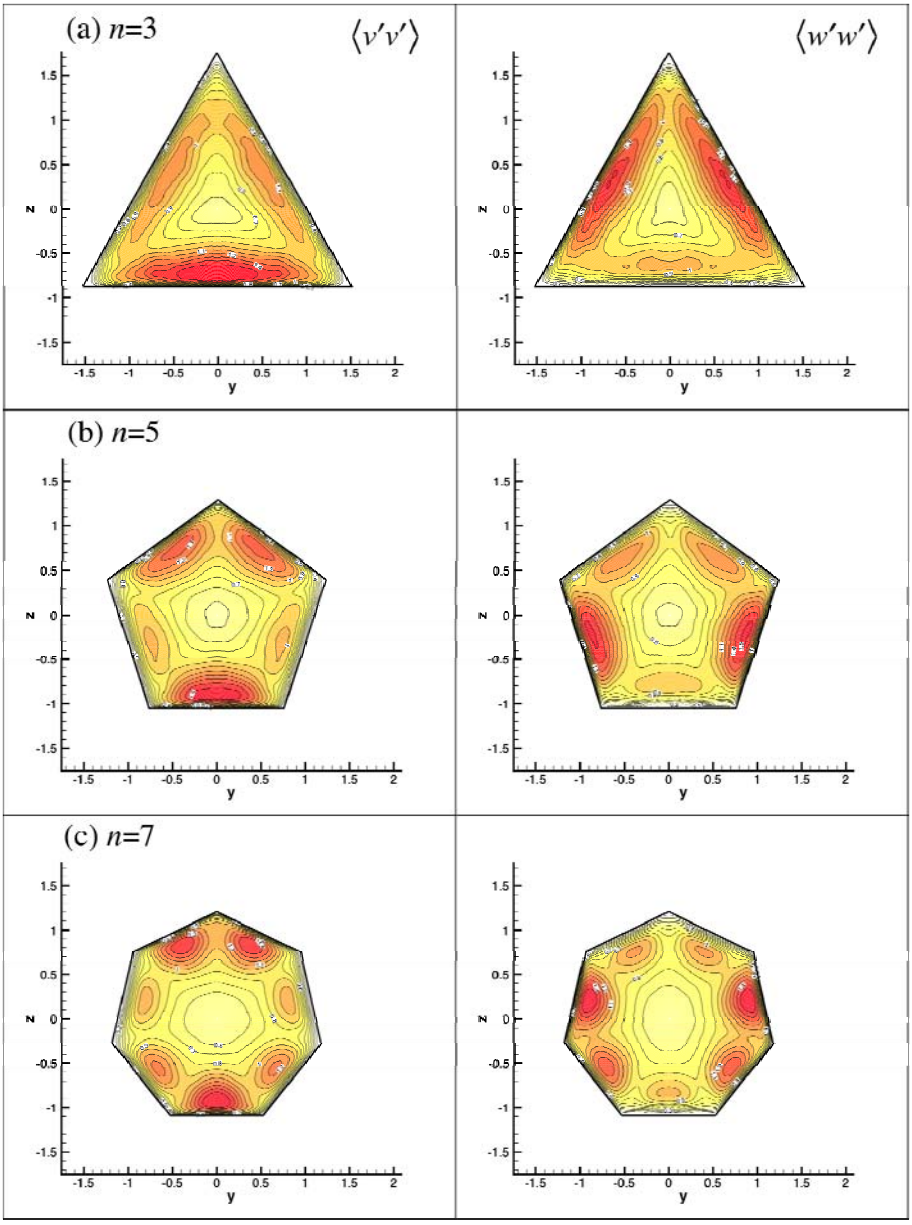

Fig. 8 Reynolds shear stresses $\langle v'v' \rangle$ and $\langle w'w' \rangle$ with odd *n*.

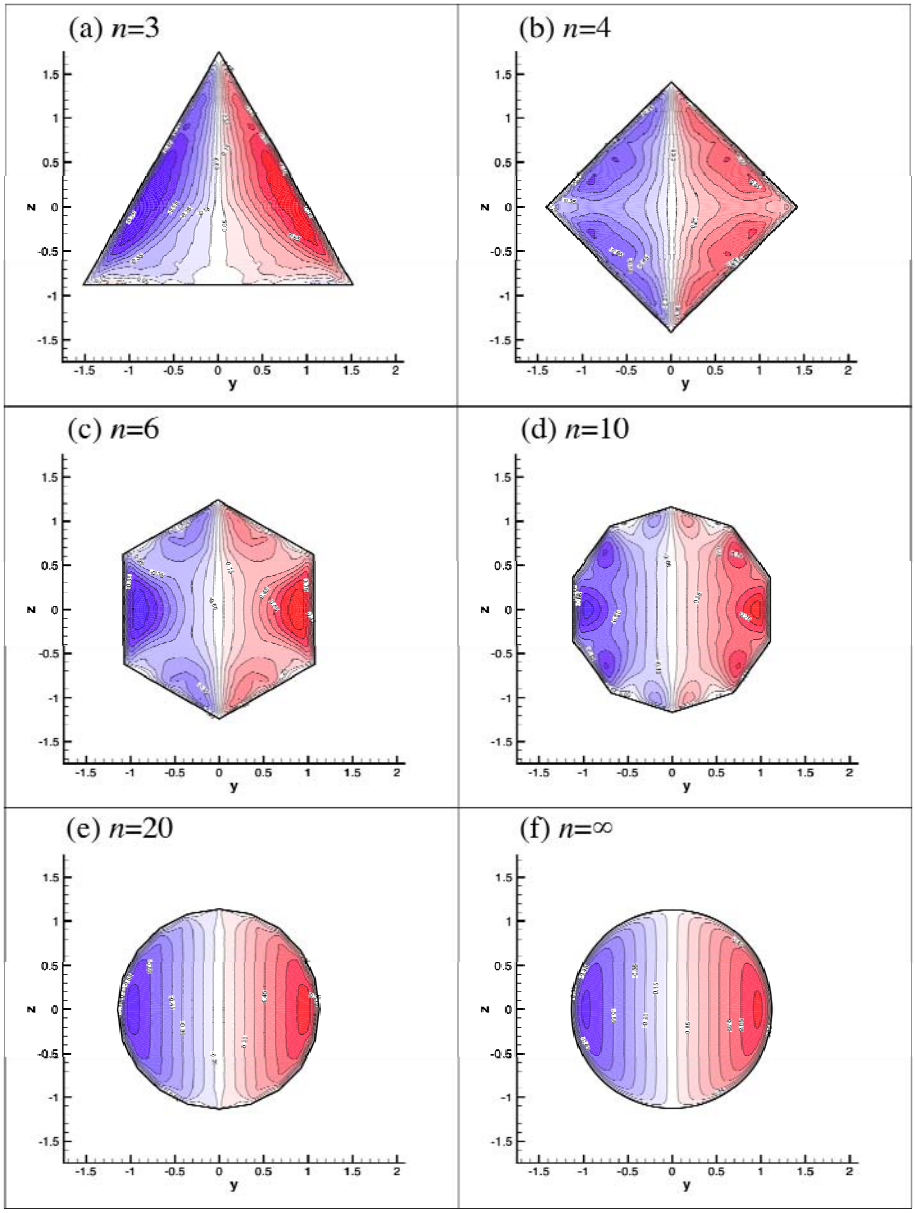

Fig. 9 Reynolds shear stress $\langle u'v' \rangle$.

regular hexagon duct shows the positive and negative large peaks near the side wall parallel to the z axis, but as n increases the regions including these peaks connect to the same-sign regions near the neighbor sides. The distribution of the regular icosagon duct is similar to that of the circular duct by eliminating the effect of each side. The relation between $\langle u'v' \rangle$ and $\langle w'u' \rangle$ is antisymmetric with $\pi/2$ rotation when n is a multiple of 4. Thus, the results of $\langle w'u' \rangle$ in the regular polygonal ducts with odd n are shown in Fig. 10 in comparison with $\langle u'v' \rangle$. $\langle w'u' \rangle$ tends to be positive at the upper region and negative at the bottom one. As n increases, the distribution of $\langle w'u' \rangle$ changes to be symmetric up and down. As can be seen in Fig. 11, in the case of all n, $\langle v'w' \rangle$ is positive in the first and third quadrants and negative in the other quadrants like a four-leaf clover. The small regions with its reverse sign appear around the clover-type distribution in the case of the equilateral triangle and regular square ducts. The small region reduces at n = 6 and 10 and the only distribution of the clover type is found in the regular icosagon and circular ducts.

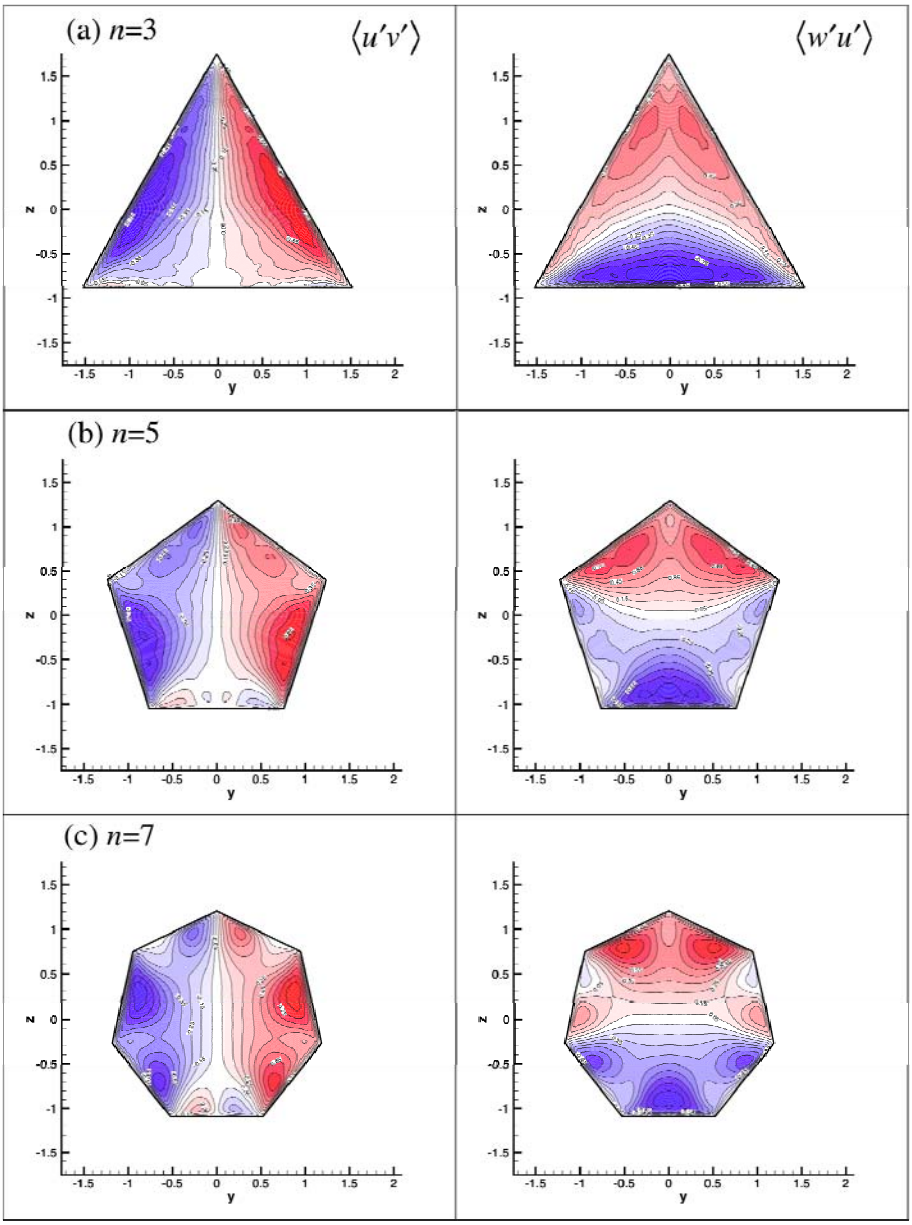

Fig. 10 Reynolds shear stresses $\langle u'v' \rangle$ and $\langle w'u' \rangle$ with odd *n*.

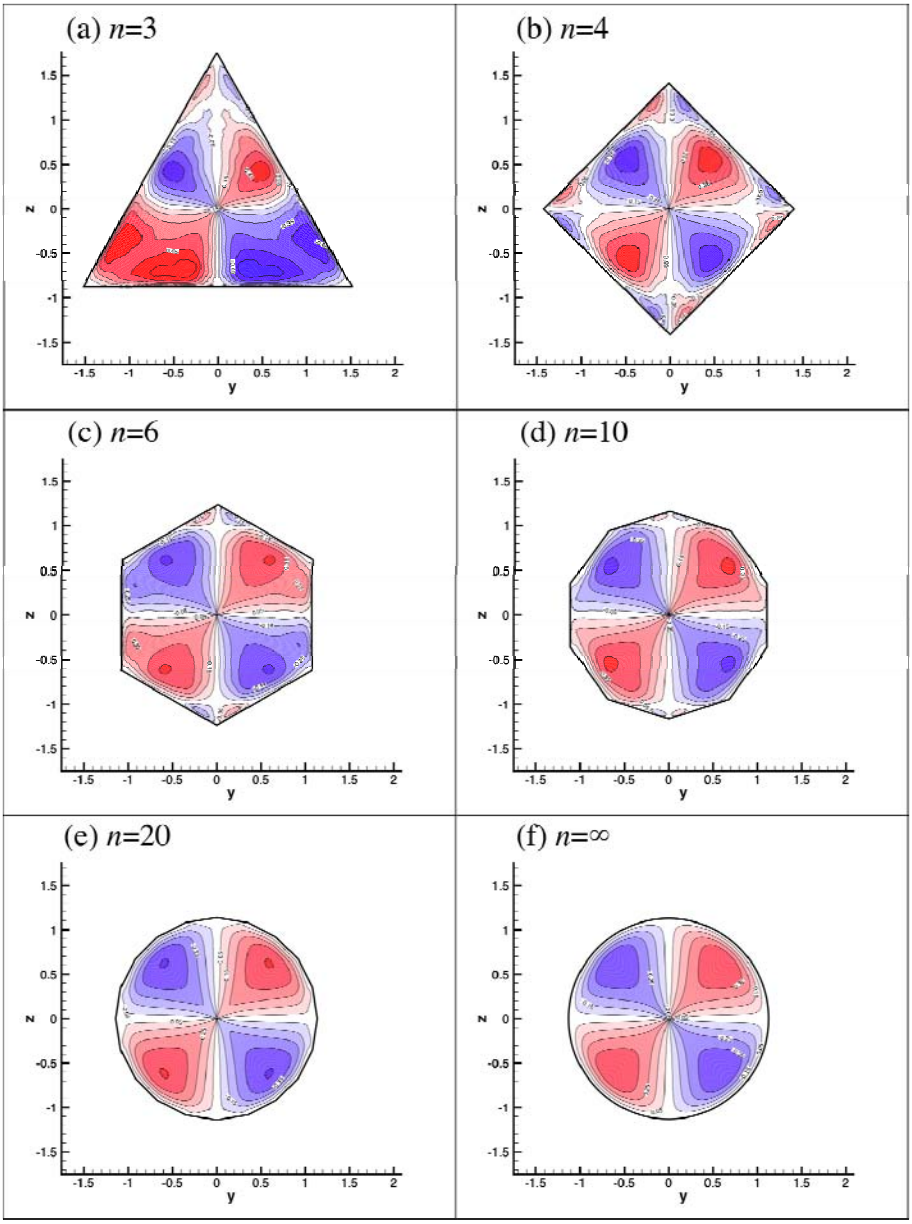

Fig. 11 Reynolds normal stress $\langle v'w' \rangle$.

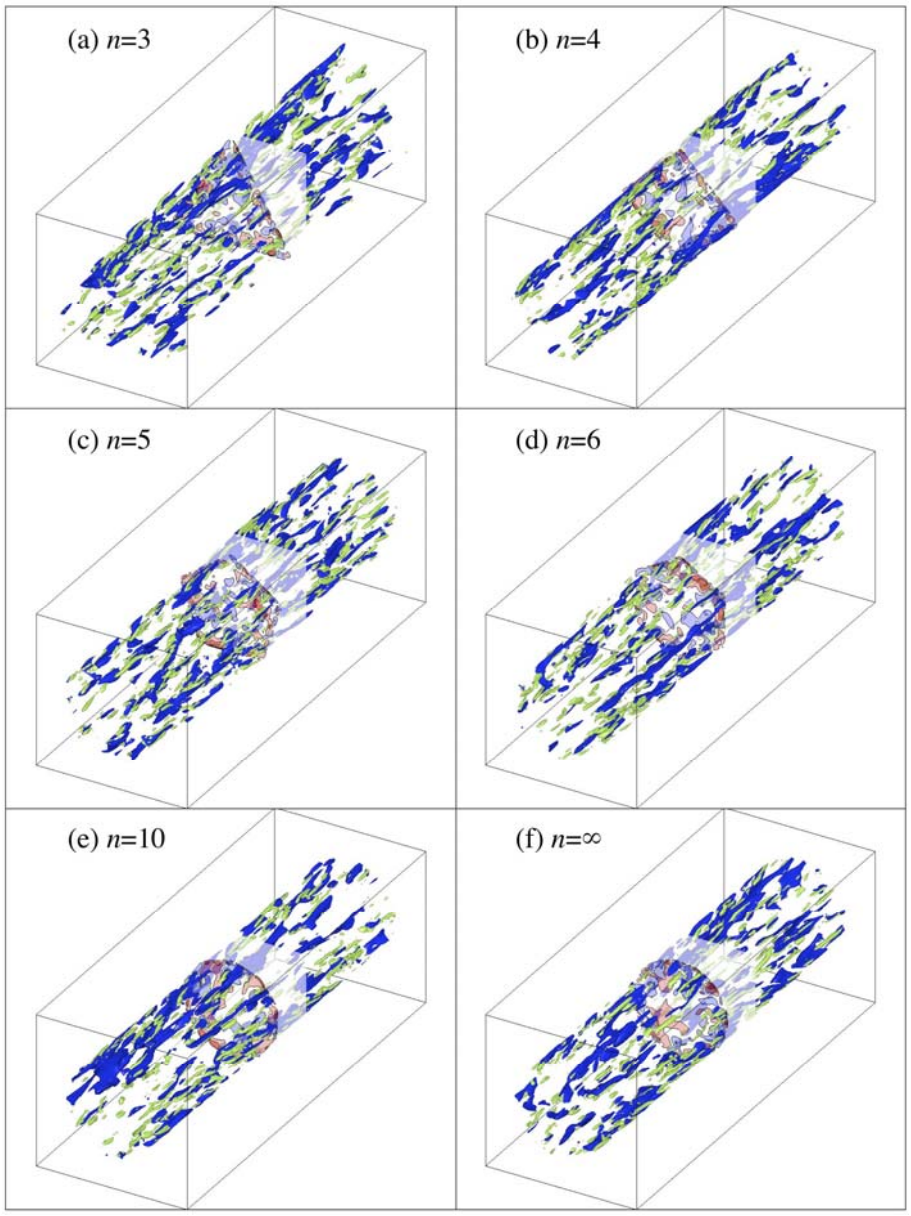

Fig. 12 Visualization of the streamwise low-speed streaks (blue region) and vortex structures (yellow one).

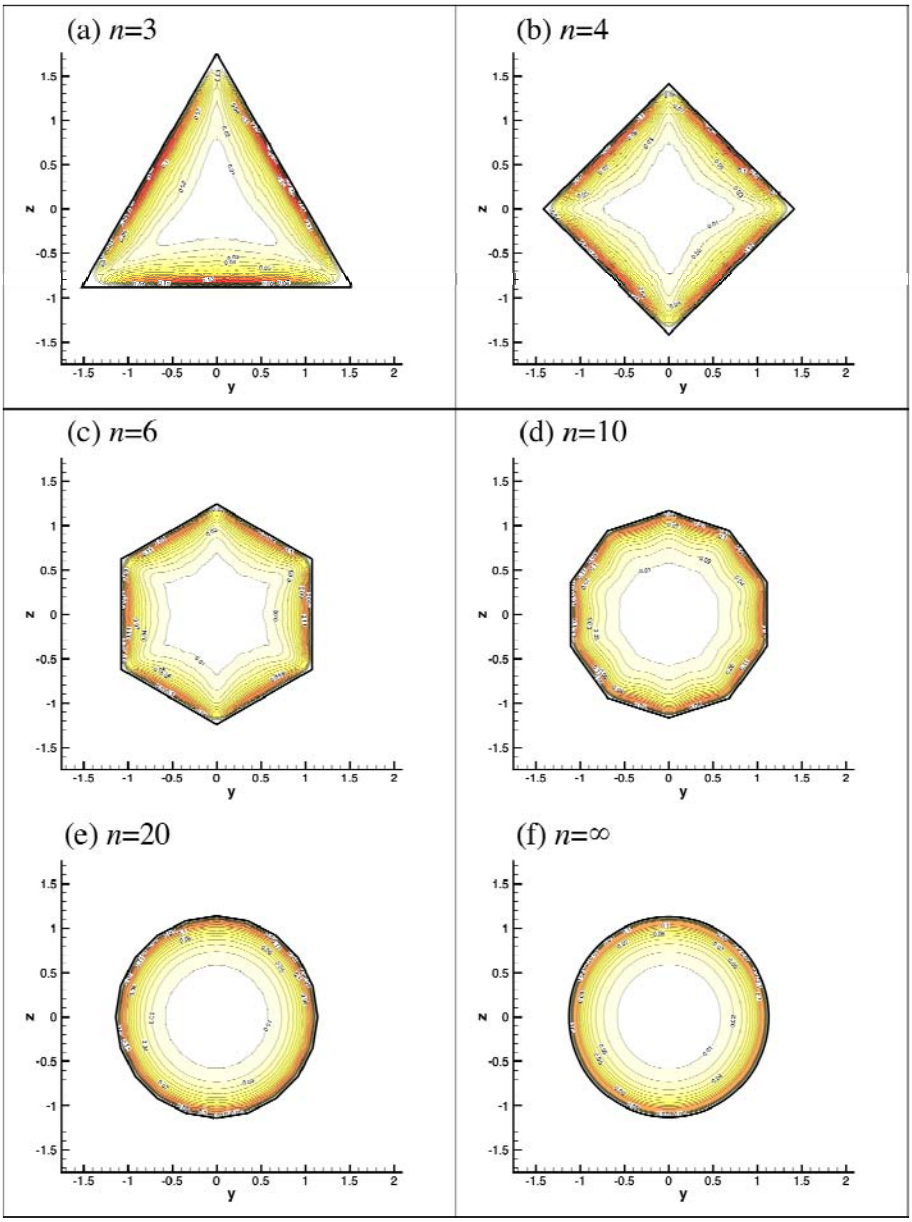

Fig. 13 Occurrence rate of the low-speed streaks.

Finally, the results of the visualization for the instantaneous field are given in Fig. 12. The low-speed streak and vortex structures are visualized by u' = -3.5 and Q_2 = 0.025 which is a second invariance of the fluctuating-velocity gradient suggested by Hunt et al. [9]. In the result of regular-pentagon and hexagon ducts the low-speed streaks tend to appear near the center region of the sides. However, the result of the regular-decagon case does not have this tendency and is similar to that of the circular case. In previous LES study [10] on the compressible channel turbulent flow, few vortex structures were detected, but a large number of vortex structures are detected in the present LES because the present resolution in the duct cross-section is very fine and about 1.4 per unit of wall coordinate. In order to estimate the low-speed streaks quantitatively, its occurrence rate is shown in Fig. 13. Few low-speed streaks occur near the vertices in the case of the regular-polygon duct with small n. As n increases, this non-occurrence region in the vicinity of vertex becomes narrow. These tendencies are also observed in the case of the vortex structures.

6. Conclusion

In this study, the numerical simulations were performed by combining the IB method with LES for fully-developed turbulent flows through 10 types of regular-polygonal ducts. In comparison of the result of the present LES with those of the DNS and the LES without the IB method with respect to the turbulent flow through the square duct, these were shortcomings in predicting the quantities related only to the streamwise mean velocity, but the present LES could reproduce the secondary flow and its related Reynolds stresses of the DNS accurately. Therefore, putting emphasis on the secondary flow in the turbulent flows through the regular-polygonal ducts, the following findings were obtained from these results. As the number of sides of the regular polygonal increases, the maximum value of the secondary flow decreases monotonously, the region of the secondary flow becomes small and appears only near the wall. In the regular-icosagon case, the secondary flow almost disappeared, and the distributions of the mean velocities and Reynolds stresses were almost the same as those in the circular pipe. There is a difference of the appearance of the turbulent coherent structures between near the vertices and the middle points of each side in the case of the regular-polygonal duct with the small number of sides, while in the case of the regular-polygonal duct with the large number of sides these behaviors almost disappeared.

In future, we will look for the cause of the underprediction of the streamwise mean velocity and try to improve the simulation code. In addition, we will investigate the effect of the Reynolds number on the relationship between the magnitude of the secondary flow and the side number of the regular-polygonal duct.

References

[1] Gavrilakis, S. 1993. “Numerical Simulation of Low-Reynolds-Number Turbulent Flow through a Straight Square Duct.” *Journal of Fluid Mechanics* 244: 101-29.

[2] Huser, A., and Biringen, S. 1993. “Direct Numerical Simulation of Turbulent Flow in a Square Duct.” *Journal of Fluid Mechanics* 257: 65-95.

[3] Okamoto, M. 2011. “Direct Numerical Simulation for Streamwise Rotating Turbulent Flow through a Square Duct.” In *Proceedings of ASME-JSME-KSME Joint Fluids Engineering Conference*, 1169-76.

[4] Umebara, M., and Okamoto, M. 2013. “Numerical Study for Compressible Turbulent Flow through a Square Duct with Different Wall Temperature.” In *Proceedings of the Symposium on Computational Fluid Dynamics*.

[5] Okabe, S., and Okamoto, M. 2018. “Mach Number Effect of Compressible Turbulent Flow through a Square Duct with Adiabatic Wall.” In *Proceedings of Mechanical Engineering Congress Japan*.

[6] Goldstein, D., Handler, R., and Sirovich, L. 1993. “Modeling a No-Slip Flow Boundary with an External Force Field.” *Journal of Computational Physics* 105: 354-66.

[7] Kobayashi, H. 2005. “The Subgrid-Scale Models Based on Coherent Structures for Rotating Homogeneous Turbulence and Turbulent Channel Flow.” *Physics of Fluids* 17: 045104.

[8] Okamoto, M. 2019. “Comparison between Incompressible and Compressible Turbulent Flows through Square Duct.” In *Proceedings of Tokai Engineering Complex*.

[9] Hunt, J. C. R., Wary, A. A., and Moin, P. 1988. “Eddies, Stream, and Convergence Zones in Turbulent Flows.” *Center for Turbulence Research Report*, 193-208.

[10] Okamoto, M., Ikemoto, A., and Sano, T. 2011. “Investigation for a One-Equation SGS Model Using DNS Data of Compressible Turbulent Channel Flow with Isothermal Walls.” *Transactions of the JSME Series B* 77 (781): 1747-57. (in Japanese)